

---

# Constrained Flow Matching via Lagrangian Dual Flows

---

Vince Kurtz  
DePaul University  
vkurtz1@depaul.edu

Alexander Davydov  
Rice University  
davydov@rice.edu

## Abstract

Flow matching is a powerful tool for generative modeling, but emerging applications in robotics, planning, and physics require inference-time constraints on generated outputs. Such constraints are often complex and highly nonlinear. As a result, methods designed for linear constraints like image inpainting are rarely sufficient, and projection or optimization-based alternatives can be prohibitively expensive. In this paper, we introduce Lagrangian Dual Flows, a new family of constrained generation techniques based on Lagrangian dual dynamics. By simply flowing a dual co-state alongside generated samples, we can guarantee nonlinear constraint satisfaction without expensive optimization subproblems, pseudoinverses, or projection steps during the denoising process. The resulting constrained generation algorithms are simple, effective, and open new theoretical connections between flow matching and primal-dual methods in numerical optimization.

## 1 Introduction

Flow matching [1] has emerged as an effective and widely-used approach for generative modeling, with applications in image and video generation [1, 2, 3], robotics [4, 5, 6], physics [7, 8], and beyond. Flow matching learns a vector field that is integrated at inference time to transport samples from a simple reference distribution (e.g., standard Gaussian) to an approximation of the data distribution.

However, many generative modeling applications require the generated output to satisfy constraints. In robotics, for example, generated actions should avoid collisions while generated trajectories must satisfy dynamic feasibility constraints. In physics-informed machine learning, generated solutions should respect underlying conservation laws. In these and many other emerging application areas, constraints are critical but (i) are only known at inference time and (ii) are often nonlinear. To meet these needs, we aim to take a pre-trained flow matching model and modify the generation procedure such that the generated samples satisfy these constraints.

Existing methods for applying inference-time constraints to a pre-trained flow-matching model either (i) require simple linear constraints [9, 10], or (ii) solve a computationally expensive subproblem at each integration step in the denoising process [11, 7]. Linear constraints are a special case of linear inverse problems, a well-studied problem class that includes image inpainting and super-resolution, but these techniques are not directly applicable to general nonlinear constraints. These and related methods often rely on computing a pseudoinverse of the constraint, which can be difficult to compute or ill-defined. Methods that support nonlinear constraints require projection to the constraint manifold [7] or the solution of optimization subproblems in each inference step [11], both of which are difficult to implement and can be computationally demanding.

Note that while linear methods are typically derived as approximate Bayesian posterior sampling, steering samples toward a conditional distribution given the constraints [9], nonlinear constrained

methods typically focus only on constraint satisfaction. We follow the latter group, and ask only that generated samples be *feasible* with respect to the constraints.

To this end, we present a family of efficient methods for constraint satisfaction in flow matching which we refer to as *Lagrangian Dual Flows* (LDF). Inspired by the classical view of constrained optimization as a continuous-time dynamical system [12, 13], we augment the state of the flow matching model with a dual variable, which plays the role of a Lagrange multiplier. The dual dynamics are a simple ordinary differential equation (ODE) defined by the constraint: the same off-the-shelf ODE integration tools typically used for flow matching can thus generate samples satisfying constraints. Our method can handle both nonlinear equality and inequality constraints and does not require any pseudoinverse or computationally expensive optimization sub-problems.

Beyond these structural advantages, LDF comes with provable guarantees. We show that the constraint violation is driven to zero at an explicit rate  $O((1-t)^\alpha)$  as  $t \rightarrow 1^-$  for an explicit constant  $\alpha > 0$ . This result holds under standard regularity and constraint-qualification assumptions, together with a small-variation condition requiring that the Gram matrix associated with the constraint Jacobian stay sufficiently close to some fixed reference matrix along the trajectory, which holds automatically for affine constraints. We emphasize that this is a guarantee of *feasibility* of the generated sample, not of convergence to any particular conditional distribution.

In summary, our contributions are as follows:

- We introduce *Lagrangian Dual Flows*, a family of methods for enforcing inference-time constraints on a pre-trained flow matching model by augmenting the generative ODE with dual (and, for inequality constraints, slack) variables. Sampling requires only the same off-the-shelf ODE solvers used for unconstrained flow matching, enabling simple and computationally efficient implementations.
- Our proposed approach supports general nonlinear equality and inequality constraints known only at inference time. Inequalities are handled via a globally Lipschitz slack reformulation whose dynamics keep the slack nonnegative automatically (Lemma 2).
- We prove that the constraint violation converges to zero as  $t \rightarrow 1^-$  with an explicit algebraic rate (Theorems 1 and 3).
- We demonstrate the effectiveness of our approach on nonlinear equality constraint, inequality constraint, and image inpainting examples, showing tighter constraint satisfaction than pseudoinverse and penalty-based baselines, with substantially lower integration cost than optimization/projection-based methods.

The remainder of this paper is organized as follows: Section 2 reviews existing methods for constrained flow matching, while Section 3 presents background and a formal problem setting. Section 4 presents our main results, including algorithms for equality and inequality-constrained generation and theoretical convergence analysis. We illustrate the effectiveness of LDF with several examples in Section 5, provide a detailed discussion of limitations and future work in Section 6, and provide conclusions in Section 7.

## 2 Related Work

Given the importance of constraints in many applications, inference-time constrained flow matching is an area of rapid research and development. Here we briefly review key methods in this area.

**Penalty and guidance with quadratic costs.** A large family of training-free methods steers a pre-trained diffusion or flow matching model toward a constraint by adding the gradient of a quadratic constraint-violation penalty to the ODE dynamics. Reconstruction guidance in video diffusion [2], manifold-constrained gradients [14], and pyramidal denoising [15] are all examples of this approach. The guidance of flow matching has received a more comprehensive treatment in [16]. Such corrections are inherently soft; since the guidance term needs to balance the pre-trained drift, constraint satisfaction is only ever approximate. Tighter constraint satisfaction requires a larger penalty, which in turn makes the denoising ODE stiffer and more difficult to integrate. In our proposed approach, we include a penalty term that plays the same role, but it is augmented by a flowed dual variable that drives the residual to zero exactly while limiting numerical ill-conditioning.

**Pseudoinverse and posterior sampling guidance.** A second family of methods for constraint satisfaction approximates the conditional score through a Gaussian posterior. This approach yields corrections built from the pseudoinverse of the constraint Jacobian. Pseudoinverse-guided diffusion (IIGDM) [9] enforces linear measurements in this way. Subsequent work refines the posterior covariance [17] and adapts the approach to flow models for linear inverses [10, 18] and diffusion posterior sampling [19]. In robotics, real-time action-chunking policies use pseudoinverse guidance to constrain initial generated actions [20]. These methods are designed for Bayesian posterior sampling under (approximately) linear-Gaussian measurement models, and the per-step pseudoinverse cost scales with the number of constraints. Our approach includes a dual correction term that recovers a similar structure when specialized to linear constraints (see Section 4.1), but we replace the explicit pseudoinverse with a dual variable with simple ODE dynamics.

**Projection and reflection-based methods.** A third family of methods enforces constraints geometrically, by projecting intermediate or terminal iterates onto the feasible set or by reflecting the dynamics at the boundary of this set. Gradient-free hard-constrained sampling [21] alternates projection-style correction steps with the generative update, while reflected Schrödinger bridges [22] and reflected flow matching [23] restrict trajectories to a domain by reflect samples at the constraint boundary. Physics-constrained flow matching (PCFM) projects each step via a full forward-backward ODE solve [7]. More recently, PolyFlow [24] embeds polyhedral constraints directly into the model architecture, using a ray-shooting operation to keep each update within the feasible set by construction and thereby avoiding projection or optimization solves at inference time. These approaches are effective for simple or convex constraints where projection is computationally cheap, but exact projection onto a general nonlinear constraint set is itself an optimization problem, and hard projection inside an ODE yields a discontinuous, projected dynamical system [25]. Our dual/slack formulation avoids these complexities: the soft-projected dynamics in Section 4.4 keep the dynamics globally Lipschitz and preserve the non-negativity of slack variables automatically.

**Control-theoretic methods.** A fourth family of methods borrows machinery from trajectory optimization, model predictive control, and control barrier functions (CBFs). HardFlow enforces hard constraints through non-convex trajectory optimization [11]. Certified motion planners combine flow matching with CBF or quadratic-program-based safety filters [26, 27, 28]. These methods ensure tight constraint satisfaction but solve an optimization subproblem at every integration step, which dominates their cost. Additionally, proper use of CBFs requires finding a Lyapunov-like barrier function compatible with both the constraint and the system dynamics [29]. This can pose a considerable challenge when the dynamics are defined by a large pre-trained flow matching model.

**ODE-based optimization.** Finally, our proposed approach draws on the classical view of optimization algorithms as dynamical systems. The basic differential multiplier method of Platt and Barr [13] evolves primal and dual variables jointly along an ODE whose equilibria are the constrained stationary points of this equality-constrained optimization problem. Continuous-time saddle-point and primal-dual flows remain a useful tool for analyzing and designing optimization algorithms [12, 30, 31, 32]. LDF leverages these idea for generative modeling: rather than running a primal-dual flow to convergence as a separate optimization procedure for constraining the generated sample, we couple the dual dynamics to the generative ODE and integrate both with the same off-the-shelf solver so that constraint satisfaction is achieved at the conclusion of the generation process.

### 3 Background

*Generative modeling and flow matching.* The goal of generative modeling is to draw new samples from an unknown data distribution  $\mathcal{D}$  on  $\mathbb{R}^n$  given access only to a finite collection of samples  $x^{(i)} \sim \mathcal{D}, i \in \{1, \dots, N\}$ . Flow matching [1] approaches this challenge by learning a time-varying vector field  $v_\theta : \mathbb{R}^n \times [0, 1] \rightarrow \mathbb{R}^n$  that transports a simple reference distribution into  $\mathcal{D}$ . Typically, a sample is generated by drawing an initial sample  $x_0$  from a standard normal distribution and integrating the ordinary differential equation

$$\dot{x}_t = v_\theta(x_t, t) \tag{1}$$

from  $t = 0$  to  $t = 1$ . The endpoint  $x_1$  is then a sample approximately distributed according to  $\mathcal{D}$ . The vector field  $v_\theta$  is trained so that its flow matches a prescribed probability path connecting the

Gaussian reference to the data. We treat  $v_\theta$  as a fixed pre-trained model and refer the reader to [1] for details on how to train a flow matching model (the subscript  $\theta$  in  $v_\theta$  denotes trainable parameters). A key feature of flow matching is that sampling requires the integration of (1), which can be performed with standard off-the-shelf ODE solvers.

*Constraints.* In many applications, the generated sample  $x_1$  is required to satisfy constraints. We consider equality and inequality constraints,

$$g(x_1) = 0, \quad h(x_1) \leq 0, \quad (2)$$

where  $g : \mathbb{R}^n \rightarrow \mathbb{R}^m$  and  $h : \mathbb{R}^n \rightarrow \mathbb{R}^k$ . We understand inequality constraints componentwise, and the constraints are permitted to be nonlinear.

Crucially, we assume that  $g$  and  $h$  are only known at inference time. A robot may encounter a new obstacle, an inpainting mask may be specified by a user, or a physical conservation law may be imposed only at deployment. The vector field  $v_\theta$  is thus generally trained without knowledge of these constraints and  $\mathcal{D}$  may be supported outside of the feasible set defined by (2). As a result, an unconstrained sample  $x_1$  may violate the constraints (2).

*Objective.* Our goal is to take a pre-trained  $v_\theta$  and, at inference time, modify the sampling process such that the generated sample satisfies the constraints. We seek a modification that satisfies three properties. First, it should certify constraint satisfaction: the generated  $x_1$  should provably satisfy (2) at least up to small numerical tolerances. Second, it should accommodate nonlinear  $g$  and  $h$ . Third, it should remain computationally lightweight, ideally requiring no more than the integration of an augmented ODE with the same off-the-shelf solvers used for unconstrained sampling. In particular, we would like to avoid solving optimization subproblems (e.g., projection onto the constraint set) or expensive nonlinear pseudoinverse computations at each integration step.

## 4 Lagrangian Dual Flows

In this section we introduce LDF, our family of methods for enforcing constraints on a pre-trained flow matching model at inference time. We begin by building intuition from two classical approaches to constrained problems. We then turn to theoretical analysis of this approach.

### 4.1 Intuition

Before formally presenting our approach, we motivate its form by examining two classical approaches to enforcing an equality constraint  $g(x) = 0$  on the output of a flow (1). Both approaches admit natural continuous-time formulations within the flow matching framework, and each has a well-known shortcoming that our proposed approach addresses.

*Penalty method.* A simple way to drive the sample toward the constraint set is to add the negative gradient of a quadratic penalty  $\frac{c}{2} \|g(x)\|^2$  to the flow:

$$\dot{x}_t = v_\theta(x_t, t) - c J_g(x_t)^\top g(x_t), \quad (3)$$

where  $c > 0$  is a constant and  $J_g(x) = \nabla_x g(x)$  is the Jacobian of  $g$ . For large  $c$ , the correction term dominates whenever  $g(x)$  is non-negligible, pulling the trajectory toward the constraint manifold  $\{x \mid g(x) = 0\}$ . However, exact constraint satisfaction requires  $c \rightarrow \infty$ : for any finite  $c$ , a residual proportional to  $1/c$  persists at  $t = 1$ , since the penalty must balance the pre-trained drift. Additionally, the ODE becomes increasingly stiff as  $c$  grows. Numerical integration then either requires very small step sizes or implicit solvers, both of which substantially increase the cost of sampling.

*Tangential projection.* A more principled approach is to require that the corrected flow remain tangent to the constraint manifold, so that trajectories never move away from  $g(x) = 0$  and do not drift off the constraint set after reaching it. To this end, consider augmenting the unconstrained flow with a correction of the form  $-J_g(x)^\top \mu$ , for some coefficient  $\mu \in \mathbb{R}^m$  to be determined:

$$\dot{x}_t = v_\theta(x_t, t) - J_g(x_t)^\top \mu. \quad (4)$$

Differentiating the constraint along this flow gives

$$\frac{d}{dt} g(x_t) = J_g(x_t) v_\theta(x_t, t) - J_g(x_t) J_g(x_t)^\top \mu. \quad (5)$$

To ensure flows are tangent to the constraint, we set  $\frac{d}{dt} g(x_t) = 0$  and choose

$$\mu(x, t) = (J_g(x) J_g(x)^\top)^{-1} J_g(x) v_\theta(x, t). \quad (6)$$

Substituting (6) back into (4) and combining with a penalty term like (3) yields

$$\dot{x}_t = (I - J_g(x_t)^\dagger J_g(x_t)) v_\theta(x_t, t) - c J_g(x_t)^\top g(x_t), \quad (7)$$

where  $J_g(x)^\dagger = J_g(x)^\top (J_g(x) J_g(x)^\top)^{-1}$  is the Moore-Penrose pseudoinverse of  $J_g(x)$  and the penalty term ensures that  $g$  converges to zero. Note that we can choose a much smaller  $c > 0$  in this case, as the multiplier  $\mu(x, t)$  eliminates movement away from the constraint manifold.

The cost of this approach is dominated by (6): every evaluation of the right-hand side requires solving an  $m \times m$  linear system with the matrix  $J_g J_g^\top$ . For applications with many constraints, e.g., long action sequences in robotics or high-dimensional inpainting masks, this cost can become prohibitive, especially when  $J_g J_g^\top$  is ill-conditioned. To avoid this, our proposed approach approximates the Lagrange multiplier  $\mu(x, t)$  without computing (6) explicitly.

## 4.2 The Proposed Method

Let  $g : \mathbb{R}^n \rightarrow \mathbb{R}^m$  be the equality constraint in (2) and let  $J_g(x) \in \mathbb{R}^{m \times n}$  denote its Jacobian matrix evaluated at  $x \in \mathbb{R}^n$ . Inspired by constrained differential optimization [13], we augment the flow matching state  $x$  with a dual variable  $\lambda \in \mathbb{R}^m$ , and evolve the pair  $(x, \lambda)$  jointly. For  $t \in [0, 1)$  and fixed constants  $c > 0, p \in [1, \infty)$ , the *Lagrangian dual flow* is the system

$$\dot{x}_t = v_\theta(x_t, t) - J_g(x_t)^\top \lambda_t - c J_g(x_t)^\top g(x_t), \quad (8a)$$

$$\dot{\lambda}_t = \frac{g(x_t)}{(1-t)^p}, \quad (8b)$$

with initial conditions  $x_0 \sim \mathcal{N}(0, I_n)$ ,  $\lambda_0 = 0$ . A constrained sample is generated by integrating (8) from  $t = 0$  to  $t = 1$  and returning  $x_1$ , as outlined in Algorithm 1 below.

---

### Algorithm 1 Equality-constrained Lagrangian Dual Flows

---

**Require:** Trained flow model  $v_\theta(x, t)$ , constraint  $g(x)$ , penalty  $c > 0$ , constant  $p \geq 1$ .

**Ensure:** Final state  $x_1$  such that  $g(x_1) = 0$ .

- 1: Initialize the state  $x_0 \sim \mathcal{N}(0, I_n)$ .
- 2: Initialize the dual  $\lambda_0 = 0$ .
- 3: Integrate from  $t = 0$  to  $t = 1$ :

$$\begin{aligned} \dot{x}_t &= v_\theta(x_t, t) - J_g(x_t)^\top \lambda_t - c J_g(x_t)^\top g(x_t), \\ \dot{\lambda}_t &= g(x_t)/(1-t)^p. \end{aligned}$$

**return**  $x_1$

---

The dynamics (8) modify the unconstrained flow (1) through two correction terms in (8a) and the introduction of an auxiliary equation (8b). First, the term  $-c J_g(x)^\top g(x)$  in (8a) pulls the sample toward the constraint set with the strength of the pull controlled by the weight  $c > 0$ . Second, the term  $-J_g(x)^\top \lambda$  applies a correction in directions normal to the constraint set with magnitude set by the dual variable  $\lambda$ . Rather than a fixed penalty or a quantity computed from  $x$ ,  $\lambda$  is a system state and is integrated over time according to the dynamics (8b). The time-rescaling factor  $(1-t)^{-p}$  makes this accumulation increasingly aggressive as  $t \rightarrow 1^-$ , concentrating the correction near the end of the integration interval. This rescaling is necessary because, unlike in [13] where integration is from  $t = 0$  to  $t = \infty$ , flow models integrate from  $t = 0$  to  $t = 1$ . The exponent  $p > 0$  governs the rate of this concentration: its choice is the subject of our theoretical analysis in Section 4.3. Intuitively, growth in  $(1-t)^{-p}$  is balanced by decay in  $g(x_t)$  during the integration process.

*Computational cost.* Sampling from (8) only requires the integration of an augmented ODE, carried out with the same off-the-shelf integrators used for unconstrained flow matching. Compared to unconstrained flow matching, LDF adds  $m$  scalar ODE channels for the dual variables and, per evaluation of the right-hand-side, a single vector-Jacobian product (VJP)  $[\lambda_t + c g(x_t)]^\top J_g(x_t)$ . This VJP is cheaply available via automatic differentiation. Importantly, LDF does not require the construction of any pseudoinverse or optimization subproblem at each integration step.

### 4.3 Theoretical Analysis

We now establish that LDF drives the equality constraint violation to zero as  $t \rightarrow 1^-$ . We defer discussion of inequality constraints to Section 4.4. Our analysis rests on the following standing assumptions, which we take to hold along the trajectory of the dynamics (8).

- (A1) *Smoothness*:  $g \in C^2(\mathbb{R}^n; \mathbb{R}^m)$  and  $v_\theta \in C^1(\mathbb{R}^n \times [0, 1]; \mathbb{R}^n)$ , and there exist constants  $L, B \geq 0$  such that  $\|J_g(x)\|_2 \leq L$  and  $\|v_\theta(x, t)\| \leq B$  along the trajectory.
- (A2) *Constraint qualification*: There exist constants  $0 < a_{\min} \leq a_{\max} < \infty$  such that  $a_{\min} I_m \preceq J_g(x)J_g(x)^\top \preceq a_{\max} I_m$  along the trajectory.
- (A3) *Bounded trajectory*: The trajectory  $(x_t, \lambda_t)$  exists on  $[0, 1)$  with  $x_t$  contained in a compact set.

Assumption (A1) is a standard regularity condition. Assumption (A2) is a uniform full-rank constraint qualification condition on the constraint Jacobian, ensuring that the constraint directions remain well-conditioned along the trajectory. Assumption (A3) rules out finite-time blowup.

*The role of the exponent  $p$ .* The choice of the time-rescaling exponent  $p$  in (8b) governs the asymptotic behavior of the constraint violation as  $t \rightarrow 1^-$ . We focus on  $p = 2$ , which yields exact convergence under the assumptions above, and summarize the behavior for other values of  $p$  at the end of this section and provide more details in Appendix C.

*Main result ( $p = 2$ ).* Before stating the theorem, we describe the change of variables underlying the analysis. The singularity of (8b) at  $t = 1$  is naturally handled by passing to the time variable  $\tau := -\log(1 - t)$ , which maps  $[0, 1)$  onto  $[0, \infty)$ , together with the rescaled dual variable  $\eta := (1 - t)\lambda$ . In these variables convergence as  $t \rightarrow 1^-$  corresponds to convergence as  $\tau \rightarrow \infty$ . The analysis then proceeds by constructing a Lyapunov function for the pair  $(g, \eta)$  and applying the comparison lemma [33, Lemma 3.4] to obtain an explicit convergence rate. The construction additionally requires a condition controlling the variation of the constraint Jacobian.

- (A4) *Small variation*: There exists a reference matrix  $A_* \succ 0$  such that, along the trajectory,  $\rho := K_{A_*} \sup_t \|J_g(x_t)J_g(x_t)^\top - A_*\|_2 < 1$ , where  $K_{A_*} = \|A_*^{-1} + \frac{1}{2}I\|_2 + 1$ .

We note that Assumption (A4) holds automatically with  $\rho = 0$  for affine constraints, where  $J_g(x)J_g(x)^\top$  is constant.

**Theorem 1** (Convergence at  $p = 2$ ). *Under Assumptions (A1)–(A4) and with  $p = 2$ , the trajectory of (8a)–(8b) satisfies*

$$\|g(x_t)\| \rightarrow 0 \quad \text{and} \quad (1 - t)\|\lambda_t\| \rightarrow 0 \quad \text{as } t \rightarrow 1^-.$$

*Moreover, the convergence is at an explicit algebraic rate. With  $\alpha := (1 - \rho)/\lambda_{\max}(P) > 0$ , where  $\rho < 1$  is the small-variation constant of (A4),  $\lambda_{\max}(P)$  is the largest eigenvalue of the symmetric matrix  $P = \begin{pmatrix} 2A_*^{-1} + I_m & -I_m \\ -I_m & I_m + A_* \end{pmatrix}$ , and  $A_*$  is the reference matrix from (A4), we have convergence at the rate,*

$$\|g(x_t)\| = O((1 - t)^\alpha) \quad \text{and} \quad (1 - t)\|\lambda_t\| = O((1 - t)^\alpha) \quad \text{as } t \rightarrow 1^-.$$

In particular, for affine constraints the conclusions of Theorem 1 hold without Assumption (A4).

We conclude this section with several remarks on convergence properties for different values of  $p \in [1, \infty)$ . More details are available in Appendix C.

For  $p \in [1, 2)$ , we are unable to establish constraint satisfaction under the dynamics (8). In Proposition 5 we prove the residual  $\|g(x_t)\|$  converges to a limit as  $t \rightarrow 1^-$ , but this limit is generally nonzero, so exact constraint satisfaction is not achieved. Indeed, for  $p = 1$ , we showcase a simple scalar system which converges to a nonzero value of the residual as  $t \rightarrow 1^-$ .

For  $p > 2$ , we do not have a general proof of constraint satisfaction although numerical experiments indicate convergence. In Appendix C.2, we analytically show that a simple scalar system exhibits constraint satisfaction with  $p > 2$ . However, the dynamics become increasingly difficult to integrate as  $t \rightarrow 1^-$  because  $(1 - t)^{-p}$  grows increasingly rapidly. Therefore, we suggest  $p = 2$  as a reasonable tradeoff between constraint satisfaction and ease of integration.

#### 4.4 Inequality Constraints

We now extend the method to inequality constraints  $h(x) \leq 0$ . The extension is via a standard slack-variable reformulation, with one modification that keeps the resulting dynamics Lipschitz continuous. We convert the inequality  $h(x) \leq 0$  into an equality by introducing a slack variable  $s \in \mathbb{R}^k$  and writing

$$h(x) + s = 0, \quad s \geq 0,$$

so that  $h(x) + s = 0$  together with  $s \geq 0$  recovers  $h(x) \leq 0$ . Treating  $\tilde{g}(x, s) := h(x) + s$  as an equality constraint on the augmented state  $(x, s)$  and applying the dual flow of Section 4.2 would yield dynamics for  $(x, s, \lambda)$  analogous to (8). The difficulty is the nonnegativity requirement  $s \geq 0$ : the slack dynamics produced this way do not keep  $s$  nonnegative on their own, and enforcing  $s \geq 0$  by hard projection in the ODE turns the dynamics into a projected dynamical system [25], which is discontinuous.

*Soft projection.* We instead enforce  $s \geq 0$  through a Lipschitz relaxation. The resulting Lagrangian dual flow for inequality constraints is

$$\dot{x}_t = v_\theta(x_t, t) - J_h(x_t)^\top \lambda_t - c J_h(x_t)^\top (h(x_t) + s_t), \quad (9a)$$

$$\dot{s}_t = c \left[ -s_t + \text{ReLU} \left( -h(x_t) - \frac{1}{c} \lambda_t \right) \right], \quad (9b)$$

$$\dot{\lambda}_t = \frac{h(x_t) + s_t}{(1-t)^p}, \quad (9c)$$

with  $x_0 \sim \mathcal{N}(0, I_n)$ ,  $\lambda_0 = 0$ ,  $s_0 \geq 0$ , and  $\text{ReLU}(y) = \max(y, 0)$ . The slack equation (9b) is a globally Lipschitz relaxation of the projected dynamics. This form is the continuous-time analog of a projected-gradient step on the slack variable with step size  $1/c$ . This approach is inspired by work on continuous-time projected and proximal gradient dynamics [34, 35, 36].

The resulting inference procedure is summarized in Algorithm 2 below. Again we obtain a single ODE that is integrated from  $t = 0$  to  $t = 1$ : the same off-the-shelf ODE tools used for unconstrained generation can be used for constrained generation.

---

#### Algorithm 2 Inequality-constrained Lagrangian Dual Flows

---

**Require:** Trained flow model  $v_\theta(x, t)$ , constraint  $h(x)$ , penalty  $c > 0$ , constant  $p \geq 1$ .

**Ensure:** Final state  $x_1$  such that  $h(x_1) \leq 0$ .

- 1: Initialize the state  $x_0 \sim \mathcal{N}(0, I_n)$ .
- 2: Initialize the slack  $s_0 = \max\{-h(x_0), 0\}$ .
- 3: Initialize the dual  $\lambda_0 = 0$ .
- 4: Integrate from  $t = 0$  to  $t = 1$ :

$$\dot{x}_t = v_\theta(x_t, t) - J_h(x_t)^\top \lambda_t - c J_h(x_t)^\top (h(x_t) + s_t),$$

$$\dot{s}_t = c \left[ -s_t + \max \left( -h(x_t) - \frac{1}{c} \lambda_t, 0 \right) \right],$$

$$\dot{\lambda}_t = (h(x_t) + s_t)/(1-t)^p.$$

**return**  $x_1$

---

These dynamics have a useful property: nonnegativity of the slack is preserved automatically, with no projection step and no parameters beyond those already present in the equality-constrained case.

**Lemma 2** (Positive invariance). *Along the slack dynamics (9b) with  $s_0 \geq 0$ , the slack satisfies  $s_t \geq 0$  for all  $t \in [0, 1)$ .*

*Convergence.* Under similar assumptions as in the equality-constrained case, but now imposed on  $h$  in place of  $g$  (see Assumptions (B1)-(B4) in Appendix B for specifics), we establish the soft-projected dynamics drive the inequality constraint to satisfaction as  $t \rightarrow 1^-$ .

**Theorem 3** (Convergence for inequality constraints at  $p = 2$ ). *Suppose assumptions (B1)-(B4) of Appendix B hold: smoothness, constraint qualification, a bounded-trajectory condition, and the*

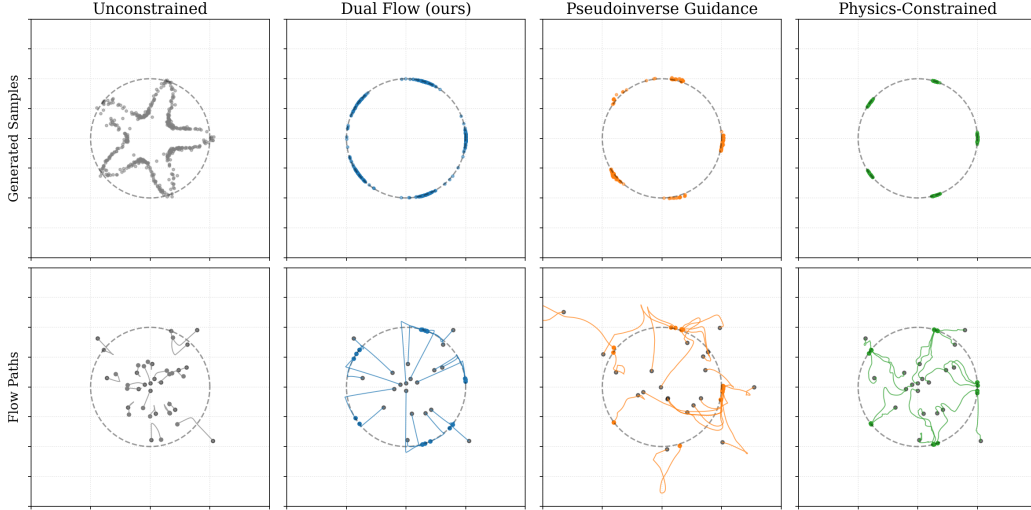


Figure 1: Generated star examples subject to a unit circle constraint. Compares our approach, pseudoinverse guidance [10], and physics-constrained flow matching [7].

*small-variation condition* (30). In particular, (B4) fixes a reference matrix  $A_*$  with dissipation margin  $\kappa_0$ . Then with  $p = 2$ , the soft-projected dynamics (9a)-(9c) satisfy

$$\|\text{ReLU}(h(x_t))\| \rightarrow 0 \quad \text{as } t \rightarrow 1^-,$$

at an explicit algebraic rate: with  $\alpha := (\kappa_0 - \rho)/\lambda_{\max}(P) > 0$ , where  $\rho < \kappa_0$  by (30) and  $\lambda_{\max}(P)$  is the maximal eigenvalue of the positive definite matrix defining the Lyapunov function of Lemma 4,

$$\|\text{ReLU}(h(x_t))\| = O((1-t)^\alpha) \quad \text{and} \quad (1-t)\|\lambda_t\| = O((1-t)^\alpha) \quad \text{as } t \rightarrow 1^-.$$

That is, the generated sample becomes feasible in the limit. For affine constraints  $h(x) = Hx + d$ , condition (B4) holds automatically and the conclusion follows from (B1)-(B3) alone.

Notably, the constraint qualification (B2) is required only on  $J_h(x)J_h(x)^\top$  itself, and the convergence matches the equality case. In particular, the soft projection contributes a controlled perturbation that vanishes as  $c \rightarrow \infty$ , as detailed in Appendix B.

*Combined constraints.* In applications it is common to impose equality and inequality constraints simultaneously. Both constraint families are handled at once by stacking them. Writing the combined constraint as  $G(x, s) := (g(x), h(x) + s)$  with separate dual variables for each family, the dynamics combine the equality flow of Section 4.2 with the soft-projected slack flow above.

## 5 Numerical Results

To test the effectiveness of our proposed approach, we implemented algorithms 1 and 2 in JAX, using FLAX/NNX for neural networks and Diffjax [37] for ODE integration. All experiments were performed on an NVIDIA RTX Pro 2000 laptop GPU (8GB). Code is available at [https://github.com/vincekurtz/constrained\\_flow\\_matching](https://github.com/vincekurtz/constrained_flow_matching).

### 5.1 Star with Unit Circle Constraint

We first consider a simple example with nonlinear equality constraints. In particular, we pre-train a small feed-forward network to generate samples from a star-shaped distribution, shown in the leftmost column of Fig. 1. We then impose a unit circle constraint

$$g(x) = \|x\|^2 - 1.$$

Example	Denosing Steps	Method	Generation Time (ms)	Constraint Violation
Star	10	Pseudoinverse [10]	2.05	$1.2 \times 10^{-2}$
Star	10	PCFM [7]	7.50	$4.2 \times 10^{-8}$
Star	10	Dual Flows (ours)	<b>1.45</b>	$3.3 \times 10^{-2}$
Star	100	Pseudoinverse [10]	17.57	$3.1 \times 10^{-2}$
Star	100	PCFM [7]	54.48	$3.0 \times 10^{-8}$
Star	100	Dual Flows (ours)	<b>9.33</b>	$2.6 \times 10^{-3}$
MNIST	10	Pseudoinverse [10]	56.22	$1.2 \times 10^0$
MNIST	10	PCFM [7]	191.82	$6.0 \times 10^{-8}$
MNIST	10	Dual Flows (ours)	<b>18.5</b>	$3.1 \times 10^{-1}$
MNIST	100	Pseudoinverse [10]	533.43	$1.1 \times 10^{-1}$
MNIST	100	PCFM [7]	1919.91	$1.0 \times 10^{-7}$
MNIST	100	Dual Flows (ours)	<b>183.31</b>	$4.9 \times 10^{-2}$

Table 1: Mean generation time and constraint violation across 20 samples from the unit-circle-constrained star (Fig. 1) and MNIST inpainting (Fig. 5).

Figure 1 compares constrained samples generated with LDF to those generated using pseudoinverse guidance [10] and PCFM [7]. For pseudoinverse guidance, which is designed for linear constraints only, we linearize the constraint about  $x_t$  at each denoising step. All methods use 100 steps ( $dt = 0.01$ ) of the second-order midpoint rule for integration: further details can be found in Appendix A.

All methods produce samples on or near the constraint manifold. However, plotting the paths of generated samples illustrates stark differences (bottom row of Fig. 1). Our dual flow method moves samples directly toward the constraint manifold and then flows along the manifold, while the other methods take more circuitous paths.

### 5.1.1 Performance Characterization

Generation times and the resulting constraint violation are shown in Table 1. Physics-constrained flow matching [7] achieves the tightest constraint satisfaction, thanks to hard projections to the constraint manifold at each denoising step. This comes at some computational expense, however, not to mention implementation difficulty. By contrast, our dual flow method adds only a few lines of code and a single Jacobian-vector product: no expensive pseudoinverses, projections, or optimization subproblems required.

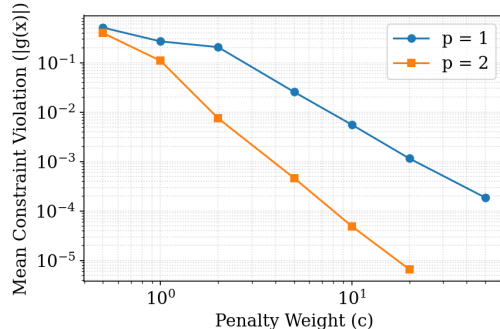


Figure 2: Average constraint violation for the star example, subject to a unit circle constraint.

### 5.1.2 Tightening Constraints

Our theoretical analysis indicates that exact constraint satisfaction is achieved (under sufficient regularity conditions) for  $p = 2$  and an exact solution of the ODE. We find that performance in practice depends on choices of coefficients  $c$  and  $p$ , as well as integration accuracy.

We investigate impact of the penalty weight  $c$  and time-rescaling factor  $p$  on constraint violation. To minimize the impact of integration errors, we use a 5th order Runge-Kutta scheme with error-controlled integration at accuracy  $10^{-5}$ , as implemented in DiffraX [37]. Figure 2 shows that constraint violation in the final generated samples decreases predictably with the penalty weight  $c$ , and that using  $p = 2$  provides tighter constraint satisfaction for the same penalty weight, though  $p = 1$  also produces reasonable performance.

### 5.1.3 Role of Lagrange Multipliers

Given the importance of the penalty coefficient  $c$ , we might wonder whether the Lagrangian dual dynamics are necessary at all. To illustrate the role of the flowed dual  $\lambda$ , we compare with a penalty-only approach where we ignore the Lagrangian term. This is similar to the quadratic penalty approach used in [2, 14]. Using error-controlled integration as above, we generate samples using a range of penalty weights  $c$ . We record the resulting constraint violation, averaged over 200 samples, and number of denoising steps required. The number of denoising steps is a rough proxy for ODE stiffness: a more difficult ODE will require more steps to resolve to the requested accuracy.

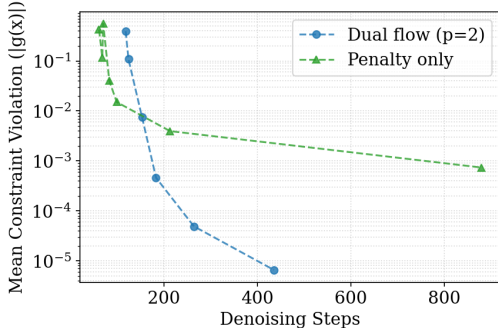


Figure 3: Comparison with a simple penalty method (e.g.,  $\lambda = 0$ ). Flowed Lagrangian dynamics allows us to further reduce constraint violations while limiting the stiffness of the ODE.

samples are shown in Fig. 4. Generating 1000 constrained samples (in parallel, 100 denoising steps, midpoint integration) takes 0.0121 seconds, compared to 0.0114 seconds for unconstrained generation.

### 5.3 MNIST Image Inpainting

Image inpainting, where only a certain subset of pixels are generated by a pre-trained model, is a special case of equality constraints  $g(x) = 0$ . In this case,  $g(x)$  is a linear constraint specifying the value of fixed pixels. We train a  $\sim 6$ M parameter UNet to generate MNIST digits, then apply an inpainting constraint, which fixes the top half of the image. Figure 5 shows the resulting images, with timing statistics summarized in Table 1.

Both pseudoinverse guidance [10] and our approach produce visually plausible images. Interestingly, while physics-constrained flow matching [7] produces the tightest constraint satisfaction (Table 1), clear artifacts are visible in the resulting images. This suggests that the projection substeps used in PCFM may be overly aggressive, pushing samples off of the data manifold in an attempt to enforce constraint satisfaction.

The resulting data is shown in Fig. 3. Even with the stiffest penalty  $c = 50$ , the penalty-only method is only able to reduce constraint violation to around  $10^{-3}$ . More critically, the penalty-only dynamics in this case become extremely stiff, requiring over 800 denoising steps to resolve. Meanwhile, LDF allows us to decrease constraint violations by two orders of magnitude with half the denoising steps.

### 5.2 Star with Inequality Constraints

To illustrate the effectiveness of Algorithm 2, we impose a simple inequality constraint on the pretrained star model,

$$h \left( \begin{bmatrix} x^0 \\ x^1 \end{bmatrix} \right) = -x^0,$$

which constrains generated samples to the right-hand side of the plane. The resulting sam-

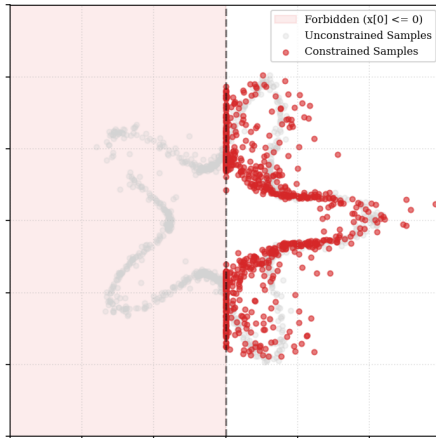


Figure 4: Samples from a pretrained “star” model, constrained to the right half of the plane using Algorithm 2.

## 6 Discussion and Limitations

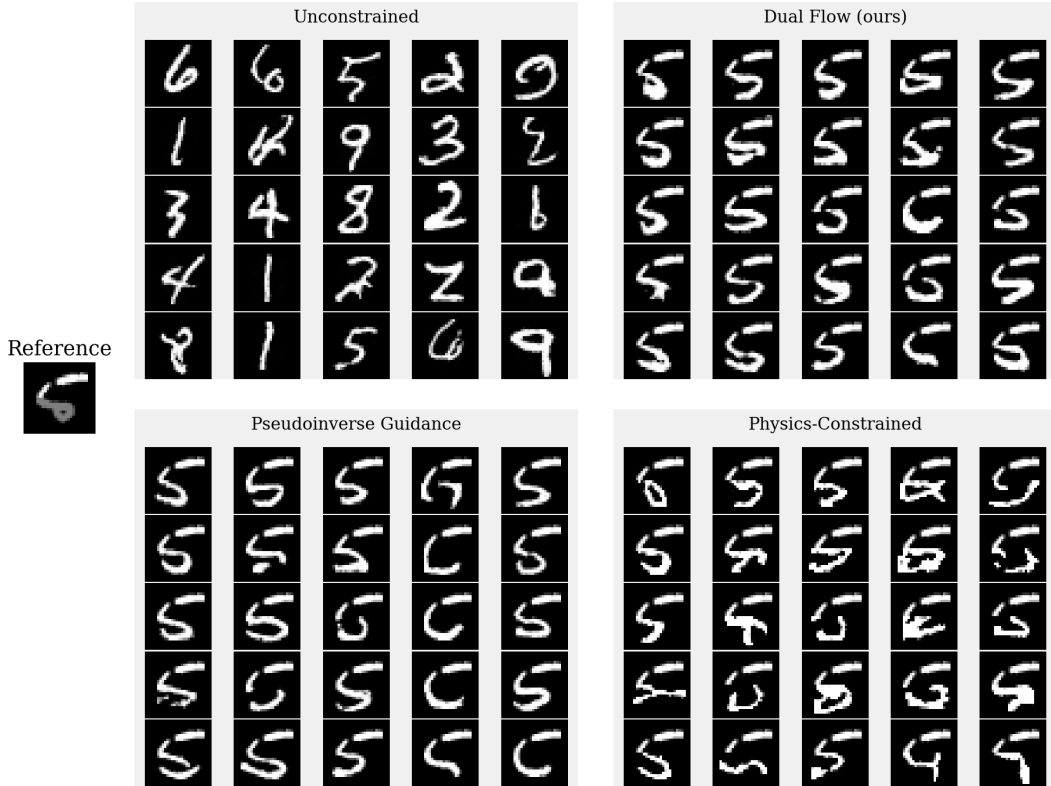


Figure 5: A pre-trained model generates MNIST handwritten digits. We then apply pseudoinverse guidance [10], physics-constrained flow matching [7], and our approach to generate new samples where the top half of the image is constrained to match the reference.

Lagrangian dual flows provide a simple, computationally efficient means to apply inference-time constraints to pre-trained flow matching policies. By flowing a dual co-state along with the samples, we can guarantee constraint satisfaction without resorting to expensive projections, pseudoinverses, or optimization subproblems. In fact, with careful implementation, a single vector-Jacobian product is all we need.

This method is designed for nonlinear equality and inequality constraints: we do not require linearity or even invertibility of the constraints. This makes LDF a promising candidate for emerging flow-matching applications like robotics, planning, and control—where constraints are critical but complex, and inference-time compute is limited.

Future work will focus on applying LDF to these domains. To this end, several challenges remain. Most importantly, LDF introduces a tradeoff between ODE stiffness and tight constraint satisfaction. Higher penalty values  $c$  produce tighter constraint satisfaction (Fig. 2), but at the cost of a stiffer ODE that may require more denoising steps to produce an acceptable result.

Additionally, LDF is concerned only with constraint satisfaction, not with generation from a new distribution that is conditioned on the constraints. As a result, constrained samples can cluster

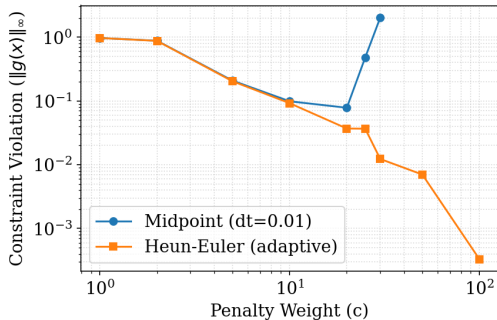


Figure 6: For MNIST image inpainting, constraint tightness saturates around  $c = 20$  with a fixed-step midpoint integrator. Error-controlled integration (in this case adaptive-step Heun-Euler) [38] allows us to further tighten constraint satisfaction.

around the constraint boundary, as shown in Fig. 4. This is a limitation shared with projection and constrained-optimization-based methods like PCFM [7]. Nonetheless, the inpainting results in Fig. 5 suggest that LDF-constrained samples are able to remain close to the data manifold, at least in certain cases.

Finally, this work opens an important bridge between flow matching and primal-dual methods in constrained optimization. Primal-dual methods enjoy a rich literature and support mature numerical implementations. Further leveraging these connections for improved inference-time-constrained flow matching remains an important and fruitful area for future research.

## 7 Conclusion

In this work, we introduced Lagrangian Dual Flows, a family of methods for enforcing inference-time constraints on pretrained flow matching models. By augmenting the generative ODE with a dual co-state (and slack variable for inequality constraints), LDF drives constraint violation to zero while avoiding pseudoinverses, projection steps, or optimization sub-problems. Sampling only requires the off-the-shelf ODE integrator already used for unconstrained generation. We proved that the constraint violation decays like  $O((1-t)^\alpha)$  as  $t \rightarrow 1^-$  for both equality and inequality constraints under regularity, constraint-qualification, and small-variation conditions which are automatically satisfied by affine constraints. Our experiments on nonlinear equality constraints, inequality constraints, and image inpainting tasks demonstrate that LDF attains constraint satisfaction at a fraction of the computational cost of optimization and pseudoinverse-based baselines.

More broadly, LDF draws a direct connection between flow matching and the classical theory of primal-dual and saddle point dynamics. We believe that the mature literature on continuous-time optimization offers tools that may translate into faster and tighter constrained generation. Pursuing this connection and moving from constraint feasibility to constraint-conditioned generation remains an exciting avenue for future work.

## References

- [1] Yaron Lipman, Ricky T. Q. Chen, Heli Ben-Hamu, Maximilian Nickel, and Matt Le. Flow matching for generative modeling. In *International Conference on Learning Representations (ICLR)*, 2023.
- [2] Jonathan Ho, Tim Salimans, Alexey Gritsenko, William Chan, Mohammad Norouzi, and David J. Fleet. Video diffusion models. *Advances in Neural Information Processing Systems (NeurIPS)*, 2022.
- [3] Yang Jin, Zhicheng Sun, Ningyuan Li, Kun Xu, Hao Jiang, Nan Zhuang, Quzhe Huang, Yang Song, Yadong Mu, and Zhouchen Lin. Pyramidal flow matching for efficient video generative modeling. In *International Conference on Learning Representations (ICLR)*, pages 23378–23402, 2025.
- [4] Kevin Black, Noah Brown, Danny Driess, Adnan Esmail, Michael Equi, Chelsea Finn, Niccolo Fusai, Lachy Groom, Karol Hausman, Brian Ichter, et al.  $\pi_0$ : A vision-language-action flow model for general robot control. *arXiv preprint arXiv:2410.24164*, 2024.
- [5] Qinglun Zhang, Zhen Liu, Haoqiang Fan, Guanghui Liu, Bing Zeng, and Shuaicheng Liu. FlowPolicy: Enabling fast and robust 3D flow-based policy via consistency flow matching for robot manipulation. In *AAAI Conference on Artificial Intelligence*, volume 39, pages 14754–14762, 2025.
- [6] Vince Kurtz and Joel W Burdick. Generative predictive control: Flow matching policies for dynamic and difficult-to-demonstrate tasks. *arXiv preprint arXiv:2502.13406*, 2025.
- [7] Utkarsh, Pengfei Cai, Alan Edelman, Rafael Gomez-Bombarelli, and Christopher Vincent Rackauckas. Physics-constrained flow matching: Sampling generative models with hard constraints. In *Advances in Neural Information Processing Systems (NeurIPS)*, 2025.

- [8] Giacomo Baldan, Qiang Liu, Alberto Guardone, and Nils Thuerey. Physics vs distributions: Pareto optimal flow matching with physics constraints. In *International Conference on Learning Representations (ICLR)*, 2026.
- [9] Jiaming Song, Arash Vahdat, Morteza Mardani, and Jan Kautz. Pseudoinverse-guided diffusion models for inverse problems. In *International Conference on Learning Representations (ICLR)*, 2023.
- [10] Ashwini Pople, Matthew J. Muckley, Ricky T. Q. Chen, and Brian Karrer. Training-free linear image inverses via flows. *Transactions on Machine Learning Research (TMLR)*, 2024.
- [11] Zeyang Li, Kaveh Alim, and Navid Azizan. HardFlow: Hard-constrained sampling for flow-matching models via trajectory optimization. *arXiv preprint arXiv:2511.08425*, 2025.
- [12] Kenneth J. Arrow, Leonid Hurwicz, and Hirofumi Uzawa. *Studies in Linear and Non-Linear Programming*. Stanford University Press, 1958.
- [13] John Platt and Alan Barr. Constrained differential optimization. In *Advances in Neural Information Processing Systems (NeurIPS)*, 1987.
- [14] Hyungjin Chung, Byeongsu Sim, Dohoon Ryu, and Jong Chul Ye. Improving diffusion models for inverse problems using manifold constraints. In *Advances in Neural Information Processing Systems (NeurIPS)*, 2022.
- [15] Dohoon Ryu and Jong Chul Ye. Pyramidal denoising diffusion probabilistic models. *arXiv preprint arXiv:2208.01864*, 2022.
- [16] Ruiqi Feng, Chenglei Yu, Wenhao Deng, Peiyan Hu, and Tailin Wu. On the guidance of flow matching. In *International Conference on Machine Learning (ICML)*, 2025.
- [17] Xinyu Peng, Ziyang Zheng, Wenrui Dai, Nuoqian Xiao, Chenglin Li, Junni Zou, and Hongkai Xiong. Improving diffusion models for inverse problems using optimal posterior covariance. *arXiv preprint arXiv:2402.02149*, 2024.
- [18] Mehrrsa Pourya, Bassam El Rawas, and Michael Unser. Flower: A flow-matching solver for inverse problems. In *International Conference on Learning Representations (ICLR)*, 2025.
- [19] Hyungjin Chung, Jeongsol Kim, Michael T. Mccann, Marc L. Klasky, and Jong Chul Ye. Diffusion posterior sampling for general noisy inverse problems. In *International Conference on Learning Representations (ICLR)*, 2023.
- [20] Kevin Black, Manuel Galliker, and Sergey Levine. Real-time execution of action chunking flow policies. *Advances in Neural Information Processing Systems (NeurIPS)*, 38:33383–33407, 2026.
- [21] Chaoran Cheng, Boran Han, Danielle C. Maddix, Abdul Fatir Ansari, Andrew Stuart, Michael W. Mahoney, and Bernie Wang. Gradient-free generation for hard-constrained systems. In *International Conference on Learning Representations (ICLR)*, 2025.
- [22] Wei Deng, Yu Chen, Nicole Tianjiao Yang, Hengrong Du, Qi Feng, and Ricky T. Q. Chen. Reflected Schrödinger bridge for constrained generative modeling. In *Uncertainty in Artificial Intelligence (UAI)*, 2024.
- [23] Tianyu Xie, Yu Zhu, Longlin Yu, Tong Yang, Ziheng Cheng, Shiyue Zhang, Xiangyu Zhang, and Cheng Zhang. Reflected flow matching. In *International Conference on Machine Learning (ICML)*, 2024.
- [24] Jianming Ma, Qiyue Yang, Yang Zhang, Liyun Yan, Zhanxiang Cao, Yazhou Zhang, and Yue Gao. PolyFlow: Safe and efficient polytope-constrained flow matching with constraint embedding and projection-free update. In *International Conference on Machine Learning (ICML)*, 2026.
- [25] Anna Nagurny and Ding Zhang. *Projected Dynamical Systems and Variational Inequalities With Applications*, volume 2. Springer Science & Business Media, 2012.

- [26] Wei Xiao, Tsun-Hsuan Wang, Chuang Gan, Ramin Hasani, Mathias Lechner, and Daniela Rus. SafeDiffuser: Safe planning with diffusion probabilistic models. In *International Conference on Learning Representations (ICLR)*, 2025.
- [27] Xiaobing Dai, Zewen Yang, Dian Yu, Fangzhou Liu, Hamid Sadeghian, Sami Haddadin, and Sandra Hirche. SafeFlow: Safe robot motion planning with flow matching via control barrier functions. *arXiv preprint arXiv:2504.08661*, 2025.
- [28] Zewen Yang, Xiaobing Dai, Dian Yu, Zhijun Li, Majid Khadiv, Sandra Hirche, and Sami Haddadin. UniConFlow: A unified constrained flow-matching framework for certified motion planning. *arXiv preprint arXiv:2506.02955*, 2025.
- [29] Aaron D Ames, Samuel Coogan, Magnus Egerstedt, Gennaro Notomista, Koushil Sreenath, and Paulo Tabuada. Control barrier functions: Theory and applications. In *European Control Conference (ECC)*, pages 3420–3431, 2019.
- [30] Diego Feijer and Fernando Paganini. Stability of primal–dual gradient dynamics and applications to network optimization. *Automatica*, 46(12):1974–1981, 2010.
- [31] Ashish Cherukuri, Bahman Ghahsifard, and Jorge Cortés. Saddle-point dynamics: Conditions for asymptotic stability of saddle points. *SIAM Journal on Control and Optimization*, 55(1):486–511, 2017.
- [32] Guannan Qu and Na Li. On the exponential stability of primal-dual gradient dynamics. *IEEE Control Systems Letters*, 3(1):43–48, 2019.
- [33] Hassan K. Khalil. *Nonlinear Systems*, volume 3. Prentice Hall, 2002.
- [34] Xing-Bao Gao. Exponential stability of globally projected dynamic systems. *IEEE Transactions on Neural Networks*, 14(2):426–431, 2003.
- [35] Sepideh Hassan-Moghaddam and Mihailo R. Jovanović. Proximal gradient flow and Douglas–Rachford splitting dynamics: Global exponential stability via integral quadratic constraints. *Automatica*, 123:109311, 2021.
- [36] Alexander Davydov, Veronica Centorrino, Anand Gokhale, Giovanni Russo, and Francesco Bullo. Time-varying convex optimization: A contraction and equilibrium tracking approach. *IEEE Transactions on Automatic Control*, 70(11):7446–7460, 2025.
- [37] Patrick Kidger. *On Neural Differential Equations*. PhD thesis, University of Oxford, 2021.
- [38] Ernst Hairer, Gerhard Wanner, and Syvert P Nørsett. *Solving Ordinary Differential Equations I: Nonstiff Problems*. Springer, 1993.
- [39] Prafulla Dhariwal and Alexander Nichol. Diffusion models beat GANs on image synthesis. In *Advances in Neural Information Processing Systems (NeurIPS)*, volume 34, pages 8780–8794, 2021.

## A Implementation Details

Our implementation of LDF, along with baselines and code for reproducing all figures in this paper, is available at [github.com/vincekurtz/constrained\\_flow\\_matching](https://github.com/vincekurtz/constrained_flow_matching). We use JAX and Flax NNX for model training and deployment; ODEs are solved with Difffrax [37].

### A.1 Constrained Generation Methods

#### A.1.1 Lagrangian Dual Flows

We implement Algorithms 1 and 2 in JAX, leaving the penalty  $c$  and dual flow exponent  $p$  as free parameters. The correction terms in (8a) are implemented using a single VJP: the explicit Jacobian  $J_g(x)$  is never formed or stored in memory.

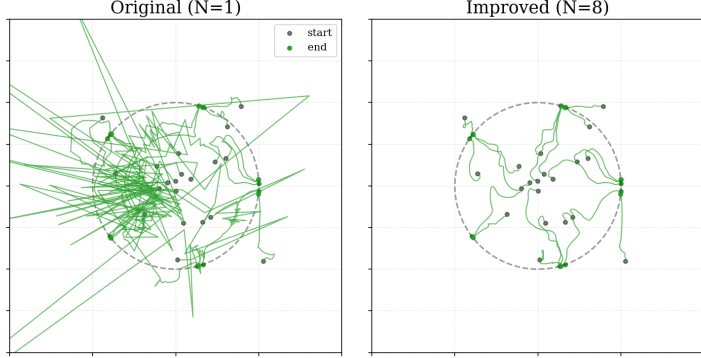


Figure 7: The original PCFM algorithm (left, [7, Algorithm 1]) produces extremely noisy generation paths for our star examples, subject to a unit circle constraint. We compare with an improved baseline (right), where increasing the number of projection steps avoids overshoot and results in more reasonable generation paths.

We wrap the dynamics of the sample  $x$ , Lagrange multipliers  $\lambda$ , and any slack variables  $s$  into a single ODE, and solve this ODE with DiffraX. For fixed-step integration, we use the second-order midpoint method. For error-controlled integration, we use DiffraX’s default step-size controller with a minimum step size of  $10^{-5}$ .

### A.1.2 Penalty Only Baseline

The penalty-only baseline (Fig. 3) exercises the same code path as our proposed approach, but we fix  $\lambda = 0$ . The net ODE is therefore

$$\dot{x}_t = v_\theta(x_t, t) - c \nabla_x \|g(x_t)\|^2, \quad (10)$$

a simple quadratic penalty guiding the generation process.

### A.1.3 Pseudoinverse Guidance Baseline

For pseudoinverse guidance, we use JAX and DiffraX to flow samples according to the ODE defined in [10, Algorithm 1]. Note that this algorithm is designed for linearly constrained problems of the form

$$Ax = y. \quad (11)$$

To support generic nonlinear constraints  $g(x) = 0$ , we simply replace  $A$  with the Jacobian  $J_g(x_t)$  and the residual  $Ax - y$  with  $g(x)$ .

To maximize runtime performance, we use LU decomposition and a linear solve to avoid full computation of the Moore-Penrose pseudoinverse, and a single VJP to avoid storing the full Jacobian of last-state predictions with respect to the current estimate.

### A.1.4 Physics-Constrained Flow Matching Baseline

We similarly implement [7, Algorithm 1] using JAX and DiffraX. This PCFM algorithm is considerably more complex, involving several interleaved steps of ODE solving, projection, and optimization subproblems. We solve the optimization subproblem [7, Algorithm 1, line 8] with 10 steps of gradient descent at learning rate 0.1. We found that PCFM’s generation paths were quite sensitive to the projection step [7, Algorithm 1, line 6]. In particular, performing this projection to a linearization of the constraint manifold resulted in extremely noisy generation paths for the unit circle constraint, as shown in Fig. 7 below.

To avoid this issue, our implementation repeats this projection step  $N$  times, re-linearizing the constraint after each projection. We found that  $N = 8$  offered a reasonable balance of performance and computation speed for our examples. We use the improved  $N = 8$  version as our baseline for all of our numerical experiments.

## A.2 Models

Here we provide a brief summary regarding our pretrained flow models: full details are available at [github.com/vincekurtz/constrained\\_flow\\_matching](https://github.com/vincekurtz/constrained_flow_matching). Note that these models and architectures are not particularly optimized or finely tuned, rather they provide a testbed for applying post-hoc constraints at inference time.

For the “star” example, our pretrained flow model  $v_\theta(x, t)$  is a simple MLP with 4 hidden layers of 64 units and swish activations. We train on 1024 data points generated on a 2D star manifold. Training this small network takes a matter of minutes on a laptop.

For MNIST inpainting, we use an encoder/decoder U-net with a (64, 128, 256) dimensional channel schedule. We use a 128-dim sinusoidal time embedding, conditioned via AdaGN [39]. This model is trained to generate unconditional samples: classification labels are not used during training. Training this model takes about 30 minutes.

## B Proofs

### B.1 Proof of Theorem 1

*Proof.* The proof has four steps. We first remove the singularity at  $t = 1$  by an exponential time change (Step 1); construct a Lyapunov function and verify its positive definiteness and its exact dissipation along the autonomous limit (Step 2); decompose its derivative along the true dynamics into the autonomous part plus two controlled corrections (Step 3); and apply the comparison lemma to the resulting inequality, obtaining an explicit decay rate (Step 4).

Throughout we abbreviate

$$A(x) := J_g(x)J_g(x)^\top \in \mathbb{R}^{m \times m}, \quad b(x, t) := J_g(x)v_\theta(x, t) \in \mathbb{R}^m.$$

**Step 1 (Exponential time change).** Introduce  $\tau := -\log(1 - t)$ , mapping  $[0, 1)$  onto  $[0, \infty)$  with  $1 - t = e^{-\tau}$  and  $d\tau/dt = e^\tau$ , and the rescaled dual variable

$$\eta(\tau) := (1 - t)\lambda(t) = e^{-\tau}\lambda. \quad (12)$$

The chain rule applied to  $g(x_t)$  along (8a) gives  $\dot{g} = J_g(x)\dot{x} = b(x, t) - A(x)\lambda - cA(x)g$ . Converting to  $\tau$ -time via  $dg/d\tau = e^{-\tau}\dot{g}$  and  $\lambda = e^\tau\eta$ ,

$$\frac{dg}{d\tau} = -A(x)\eta + e^{-\tau}[b(x, t) - cA(x)g]. \quad (13)$$

For the dual variable,  $\dot{\lambda} = g/(1 - t)^2$  gives  $d\lambda/d\tau = e^{-\tau}\dot{\lambda} = e^\tau g$ , so differentiating (12),

$$\frac{d\eta}{d\tau} = -e^{-\tau}\lambda + e^{-\tau}\frac{d\lambda}{d\tau} = -\eta + g. \quad (14)$$

Under assumption (A4), as  $\tau \rightarrow \infty$  the factor  $e^{-\tau}$  vanishes, and (13)-(14) are close to the autonomous linear system  $dg/d\tau = -A_*\eta$ ,  $d\eta/d\tau = g - \eta$ , with  $A(x)$  frozen at  $A_*$ ; the deviations  $A(x) - A_*$  and the  $e^{-\tau}$  forcing are treated as corrections in Step 3.

**Step 2 (Lyapunov function).** With the reference matrix  $A_* \succ 0$  from Assumption (A4), define the candidate Lyapunov function

$$V(g, \eta) := g^\top (A_*^{-1} + \frac{1}{2}I_m)g - g^\top \eta + \frac{1}{2}\|\eta\|^2 + \frac{1}{2}\eta^\top A_*\eta. \quad (15)$$

First, we establish that this candidate is positive definite. Stacking  $w := (g, \eta) \in \mathbb{R}^{2m}$ , we have  $V = \frac{1}{2}w^\top Pw$  with

$$P = \begin{pmatrix} 2A_*^{-1} + I_m & -I_m \\ -I_m & I_m + A_* \end{pmatrix}. \quad (16)$$

Diagonalizing  $A_* = Q \text{diag}(\mu_1, \dots, \mu_m) Q^\top$  with  $Q$  orthogonal and conjugating  $P$  by  $\text{diag}(Q, Q)$  block-diagonalizes  $P$  into  $m$  blocks

$$P_i = \begin{pmatrix} 2\mu_i^{-1} + 1 & -1 \\ -1 & 1 + \mu_i \end{pmatrix}. \quad (17)$$

Each  $P_i \succ 0$  since it is strictly diagonally dominant. Hence  $P \succ 0$ , so  $V$  is positive definite and

$$c_1(\|g\|^2 + \|\eta\|^2) \leq V(g, \eta) \leq c_2(\|g\|^2 + \|\eta\|^2), \quad c_1 := \frac{1}{2}\lambda_{\min}(P), \quad c_2 := \frac{1}{2}\lambda_{\max}(P). \quad (18)$$

*Dissipation along the autonomous limit.* Along  $dg/d\tau = -A_*\eta$ ,  $d\eta/d\tau = g - \eta$  we claim

$$\left. \frac{dV}{d\tau} \right|_{\text{autonomous}} = -\|g\|^2 - \|\eta\|^2. \quad (19)$$

Differentiating (15) term by term:

$$\begin{aligned} \frac{d}{d\tau} \left[ g^\top (A_*^{-1} + \frac{1}{2}I)g \right] &= 2g^\top (A_*^{-1} + \frac{1}{2}I)(-A_*\eta) = -2g^\top \eta - g^\top A_*\eta, \\ \frac{d}{d\tau} \left[ -g^\top \eta \right] &= -(-A_*\eta)^\top \eta - g^\top (g - \eta) = \eta^\top A_*\eta - \|g\|^2 + g^\top \eta, \\ \frac{d}{d\tau} \left[ \frac{1}{2} \|\eta\|^2 \right] &= \eta^\top (g - \eta) = g^\top \eta - \|\eta\|^2, \\ \frac{d}{d\tau} \left[ \frac{1}{2} \eta^\top A_*\eta \right] &= \eta^\top A_* (g - \eta) = g^\top A_*\eta - \eta^\top A_*\eta, \end{aligned}$$

using the symmetry of  $A_*$  for  $(A_*\eta)^\top \eta = \eta^\top A_*\eta$  and  $\eta^\top A_*g = g^\top A_*\eta$ . Summing, we are left with  $-\|g\|^2 - \|\eta\|^2$ , which is (19).

**Step 3 (Decomposition along the true dynamics).** Now differentiate  $V$  along (13)-(14), where  $A(x)$  replaces  $A_*$  and the forcing  $e^{-\tau}[b - cAg]$  is present. With  $\nabla_g V = 2(A_*^{-1} + \frac{1}{2}I)g - \eta$  and  $\nabla_\eta V = -g + \eta + A_*\eta$ , substituting and decomposing  $A(x) = A_* + (A(x) - A_*)$  gives

$$\frac{dV}{d\tau} = -\|g\|^2 - \|\eta\|^2 + R_A + e^{-\tau}R_p, \quad (20)$$

where the autonomous part is exactly (19), and

$$R_A := -2g^\top \left( A_*^{-1} + \frac{1}{2}I \right) \left( A(x) - A_* \right) \eta + \eta^\top \left( A(x) - A_* \right) \eta, \quad (21)$$

$$R_p := \left( 2g^\top \left( A_*^{-1} + \frac{1}{2}I \right) - \eta^\top \right) \xi, \quad \xi := b(x, t) - cA(x)g. \quad (22)$$

*Bound on  $R_A$ .* By Cauchy-Schwarz on each term of (21) and Young's inequality  $2\|g\|\|\eta\| \leq \|g\|^2 + \|\eta\|^2$ ,

$$\begin{aligned} |R_A| &\leq 2\|g\| \left\| A_*^{-1} + \frac{1}{2}I \right\|_2 \|A(x) - A_*\|_2 \|\eta\| + \|A(x) - A_*\|_2 \|\eta\|^2 \\ &\leq \|A(x) - A_*\|_2 \left[ \left\| A_*^{-1} + \frac{1}{2}I \right\|_2 (\|g\|^2 + \|\eta\|^2) + \|\eta\|^2 \right] \\ &\leq \left( \left\| A_*^{-1} + \frac{1}{2}I \right\|_2 + 1 \right) \|A(x) - A_*\|_2 (\|g\|^2 + \|\eta\|^2) \\ &= K_{A_*} \|A(x) - A_*\|_2 (\|g\|^2 + \|\eta\|^2), \end{aligned}$$

using  $\|\eta\|^2 \leq \|g\|^2 + \|\eta\|^2$ . By Assumption (A4),  $K_{A_*} \|A(x) - A_*\|_2 \leq \rho$ , so

$$|R_A| \leq \rho (\|g\|^2 + \|\eta\|^2). \quad (23)$$

*Bound on  $R_p$ .* The vector  $\xi$  is bounded: by (A1)-(A3),  $\|\xi\| \leq \|b\| + c\|A\|_2\|g\| \leq LB + c a_{\max} G =: M_\xi$ . Then by Cauchy-Schwarz,

$$|R_p| \leq 2\|g\| \left\| A_*^{-1} + \frac{1}{2}I \right\|_2 \|\xi\| + \|\eta\| \|\xi\| \leq K_p (\|g\| + \|\eta\|), \quad (24)$$

with  $K_p := M_\xi \max\{2\|A_*^{-1} + \frac{1}{2}I\|_2, 1\}$  depending only on  $L, B, c, a_{\max}, A_*, G$ .

*Combined inequality.* Substituting (23) and (24) into (20),

$$\frac{dV}{d\tau} \leq -(1 - \rho) (\|g\|^2 + \|\eta\|^2) + e^{-\tau} K_p (\|g\| + \|\eta\|). \quad (25)$$

**Step 4 (Comparison lemma and explicit rate).** Write  $\|w\|^2 := \|g\|^2 + \|\eta\|^2$ . Since  $\|g\| + \|\eta\| \leq \sqrt{2} \|w\|$ , the combined inequality (25) gives

$$\frac{dV}{d\tau} \leq -(1 - \rho) \|w\|^2 + e^{-\tau} K \|w\|, \quad K := \sqrt{2} K_p.$$

Set  $y := \sqrt{V} \geq 0$ . Where  $V > 0$ , using  $\|w\|^2 \geq V/c_2 = y^2/c_2$  on the dissipation term and  $\|w\| \leq \sqrt{V/c_1} = y/\sqrt{c_1}$  on the forcing term (both from (18)),

$$\frac{dy}{d\tau} = \frac{1}{2\sqrt{V}} \frac{dV}{d\tau} \leq -\alpha y + \gamma e^{-\tau}, \quad \alpha := \frac{1 - \rho}{2c_2} > 0, \quad \gamma := \frac{K}{2\sqrt{c_1}} > 0.$$

The comparison lemma [33, Lemma 3.4] then gives, for all  $\tau \geq 0$ ,

$$y(\tau) \leq y(0)e^{-\alpha\tau} + \gamma \int_0^\tau e^{-\alpha(\tau-u)} e^{-u} du = y(0)e^{-\alpha\tau} + \gamma \begin{cases} \frac{e^{-\alpha\tau} - e^{-\tau}}{1 - \alpha}, & \text{if } \alpha \neq 1, \\ \tau e^{-\tau}, & \text{if } \alpha = 1. \end{cases} \quad (26)$$

Both terms on the right of (26) decay so we can conclude that  $y(\tau) \rightarrow 0$  as  $\tau \rightarrow \infty$ .

Additionally, for all  $i \in \{1, \dots, m\}$ ,  $\lambda_{\max}(P) \geq P_i^{11} = 2\mu_i^{-1} + 1 > 1$  for a symmetric matrix, and  $2c_2 = \lambda_{\max}(P)$  with  $\rho \geq 0$ , we have  $\alpha = (1 - \rho)/\lambda_{\max}(P) < 1$  and thus there is a constant  $M > 0$  such that  $y(\tau) \leq M e^{-\alpha\tau}$  for all  $\tau \geq 0$ . Converting to original time via  $e^{-\tau} = 1 - t$  and using  $\|g(x_t)\| \leq \|w\| \leq y/\sqrt{c_1}$ ,

$$\|g(x_t)\| \leq \frac{M}{\sqrt{c_1}} (1 - t)^\alpha = O((1 - t)^\alpha) \quad \text{and} \quad (1 - t) \|\lambda_t\| = \|\eta\| = O((1 - t)^\alpha)$$

as  $t \rightarrow 1^-$ . In particular both tend to zero.  $\square$

## B.2 Proof of Lemma 2 and Theorem 3

*Proof of Lemma 2.* If the  $i$ -th component of  $s_t$ ,  $s_t^i$ , is equal to zero at some time  $t \in [0, 1]$ , then from (9b),  $s_t^i = c \operatorname{ReLU}(-h^i(x_t) - \lambda_t^i/c) \geq 0$ . Hence  $s_t^i$  cannot decrease past zero and with  $s_0 \geq 0$ , we conclude that  $s_t \geq 0$  for all  $t \in [0, 1]$ .  $\square$

For self-containedness, we reproduce the assumptions for convergence here, stated in terms of  $h$ . We assume the following hold along the trajectory of (9a)-(9c).

- (B1) *Smoothness:*  $h \in C^2(\mathbb{R}^n; \mathbb{R}^k)$  and  $v_\theta \in C^1(\mathbb{R}^n \times [0, 1]; \mathbb{R}^n)$ , with  $\|J_h(x)\|_2 \leq L$  and  $\|v_\theta(x, t)\| \leq B$ ;
- (B2) *Constraint qualification:*  $a_{\min} I_k \preceq J_h(x) J_h(x)^\top \preceq a_{\max} I_k$  for constants  $0 < a_{\min} \leq a_{\max} < \infty$ .
- (B3) *Bounded trajectory:* the trajectory  $(x, s, \lambda)$  exists on  $[0, 1]$  with  $x_t$  and  $s_t$  in a compact set.

These assumptions are identical to those assumed in the equality-constrained case with the additional assumption that the slack variable  $s_t$  evolves in a compact set. This additional assumption can be enforced by replacing the  $\operatorname{ReLU}(-h(x_t) - \lambda_t/c)$  in (9b) with  $\min\{\operatorname{ReLU}(-h(x_t) - \lambda_t/c), R\}$  for some  $R > 0$ . This enforces boundedness at the expense of enforcing the two-sided constraint  $-R \leq h(x_1) \leq 0$  for the generated sample where we understand  $-R \leq h(x_1)$  to mean that each entry of  $h(x_1)$  is greater than or equal to  $-R$ .

Unlike the equality case, the soft projection switches between active sets, so the proof rests on a Lyapunov function that dissipates simultaneously in every regime. Because the dissipation margin  $\kappa_0$  it produces enters the small-variation condition, we state it first.

First, for notation, for a subset  $\mathcal{S} \subseteq \{1, \dots, k\}$ , let  $E_{\mathcal{S}} := \operatorname{diag}(\mathbf{1}_{i \in \mathcal{S}})$  be the corresponding 0/1 diagonal matrix.

**Lemma 4.** Let  $A_* \succ 0$  and define

$$V(\tilde{g}, \eta) := \frac{1}{2} (\tilde{g}, \eta)^\top P (\tilde{g}, \eta), \quad P := \begin{pmatrix} I_k & -\frac{1}{2} I_k \\ -\frac{1}{2} I_k & A_* + \frac{1}{2} I_k \end{pmatrix}. \quad (27)$$

Then  $P \succ 0$ , and for every projector  $E = E_S$  ( $S \subseteq \{1, \dots, k\}$ ), the matrix  $M_E := \begin{pmatrix} 0 & -(A_* + E) \\ I & -I \end{pmatrix}$  satisfies

$$M_E^\top P + P M_E = \begin{pmatrix} -I & I - E \\ I - E & E - A_* - I \end{pmatrix} =: D_E \prec 0. \quad (28)$$

Consequently the dissipation margin

$$\kappa_0 := \kappa_0(A_*) := \frac{1}{2} \min_{S \subseteq \{1, \dots, k\}} \lambda_{\min}(-D_{E_S}) > 0 \quad (29)$$

is uniform over all active sets, and  $dV/d\tau \leq -\kappa_0 \left( \|\tilde{g}\|^2 + \|\eta\|^2 \right)$  along  $d\tilde{g}/d\tau = -(A_* + E)\eta$ ,  $d\eta/d\tau = \tilde{g} - \eta$ . Moreover  $\nabla_{\tilde{g}} V = \tilde{g} - \frac{1}{2}\eta$ , so  $\|\nabla_{\tilde{g}} V\| \leq \frac{\sqrt{5}}{2} \|(\tilde{g}, \eta)\|$ .

The proof of Lemma 4 is given at the end of this subsection.

With  $\kappa_0$  defined, we state the small-variation condition that replaces Assumption (A4) in the inequality setting. It is the exact analog of the equality case, with the dissipation margin  $\kappa_0$  playing the role of the constant 1 and the gradient constant  $K_{A_*} = \frac{\sqrt{5}}{2}$  established in Lemma 4:

(B4) *Small variation*: there exists a reference matrix  $A_* \succ 0$  such that along the trajectory

$$\rho := \frac{\sqrt{5}}{2} \sup_t \left\| J_h(x_t) J_h(x_t)^\top - A_* \right\|_2 < \kappa_0(A_*). \quad (30)$$

As in the equality case, (B4) holds automatically with  $\rho = 0$  for affine constraints  $h(x) = Hx + d$ : then  $J_h J_h^\top = HH^\top$  is constant, and the choice  $A_* = HH^\top$  gives  $\rho = 0 < \kappa_0$ .

*Proof of Theorem 3.* The proof follows the same four steps as the equality-constrained case (Theorem 1): an exponential time change (Step 1), a Lyapunov function with autonomous dissipation (Step 2), a decomposition of its derivative along the true dynamics (Step 3), and a comparison-lemma argument yielding an explicit decay rate (Step 4). As in the equality case, the nonlinear constraint is handled directly by working with the reference matrix  $A_*$  of the small-variation condition (30), the affine case being the special case  $\rho = 0$  (with  $A_* = J_h J_h^\top$  constant). The one new ingredient relative to the equality case is that boundedness of the rescaled dual variable, immediate from Assumption (B3) there, must here be established en route in Step 4. Mirroring the abbreviations  $A(x) = J_g J_g^\top$ ,  $b(x, t) = J_g v_\theta$  of the equality case, we set

$$A(x) := J_h(x) J_h(x)^\top, \quad b(x, t) := J_h(x) v_\theta(x, t), \quad r := \text{ReLU}\left(-h(x) - \frac{1}{c}\lambda\right), \quad (31)$$

so that the slack equation (9b) reads  $\dot{s} = c(r - s)$ .

Write  $\tilde{g}(x, s) := h(x) + s$ . By Lemma 2 and  $s_0 \geq 0$  we have  $s_t \geq 0$  for all  $t$ , hence  $\|\text{ReLU}(h(x_t))\| \leq \|\tilde{g}(x_t, s_t)\|$  and it suffices to prove  $\|\tilde{g}(x_t, s_t)\| \rightarrow 0$  as  $t \rightarrow 1^-$ . By Assumptions (B1)–(B3) we may set  $G := \sup_t \|h(x_t)\| < \infty$ ,  $S := \sup_t \|s_t\| < \infty$ , and  $\|b(x_t, t)\| \leq LB$ .

**Step 1 (Exponential time change).** Let  $\tau := -\log(1 - t)$ , so  $1 - t = e^{-\tau}$ , and  $\eta := (1 - t)\lambda = e^{-\tau}\lambda$ . Applying the chain rule to  $\tilde{g} = h + s$ ,  $\dot{\tilde{g}} = J_h(x)\dot{x} + \dot{s}$ ; substituting (9a), (9b) and converting to  $\tau$ -time via  $d\tilde{g}/d\tau = e^{-\tau}\dot{\tilde{g}}$  and  $\lambda = e^\tau\eta$ ,

$$\frac{d\tilde{g}}{d\tau} = -A(x)\eta + e^{-\tau} \left[ b(x, t) - cA(x)\tilde{g} \right] + c e^{-\tau} (r - s), \quad (32)$$

For the dual variable,  $\dot{\lambda} = \tilde{g}/(1 - t)^2$  gives, exactly as in the equality case,

$$\frac{d\eta}{d\tau} = \tilde{g} - \eta, \quad \text{and} \quad \frac{ds}{d\tau} = e^{-\tau}\dot{s} = c e^{-\tau} (r - s). \quad (33)$$

The ReLU acts componentwise; let  $\mathcal{S}(t) := \{i \mid -h^i - \frac{1}{c}\lambda^i > 0\}$  be the active set (the indices where ReLU is identity) and  $E_S := \text{diag}(\mathbf{1}_{i \in \mathcal{S}})$  the corresponding 0/1 diagonal matrix. On active

components  $r^i = -h^i - \frac{1}{c}\lambda^i$ ; substituting (using  $\lambda = e^\tau \eta$ ,  $h + s = \tilde{g}$ ) the term  $c e^{-\tau} r$  contributes  $-\eta_i$  to  $d\tilde{g}_i/d\tau$  beyond  $-A(x)\eta$ , while inactive components contribute  $r^i = 0$ . Hence

$$\frac{d\tilde{g}}{d\tau} = -\left(A(x) + E_S\right)\eta + e^{-\tau} \left[ b - c(A(x) + E_S)\tilde{g} \right] - c e^{-\tau} s_{S^c}, \quad (34)$$

where  $S^c$  is the complement of  $S$  and  $s_{S^c} = E_{S^c}s$ . As  $\tau \rightarrow \infty$  the factor  $e^{-\tau}$  vanishes, and (34) together with  $d\eta/d\tau = \tilde{g} - \eta$  approaches, in each active-set regime  $S$ , the system  $d\tilde{g}/d\tau = -(A(x) + E_S)\eta$ ,  $d\eta/d\tau = \tilde{g} - \eta$ . Freezing  $A(x)$  at a fixed reference  $A_*$  renders this autonomous; Step 2 builds a Lyapunov function for the frozen system, and Step 3 treats both the  $e^{-\tau}$  forcing and the deviation  $A(x) - A_*$  as corrections. Because the active set  $S$  may change along the trajectory, this is a linear switching system and this Lyapunov function must dissipate simultaneously in every regime.

**Step 2 (Lyapunov function).** Let  $A_* \succ 0$  be the reference matrix of the small-variation condition (30), and take the Lyapunov function  $V$  of Lemma 4 built from  $A_*$ . Write  $z := (\tilde{g}, \eta)$  so that  $\|z\|^2 = \|\tilde{g}\|^2 + \|\eta\|^2$ . By Lemma 4,  $P \succ 0$ , so  $V$  is positive definite and, with  $c_1 := \frac{1}{2}\lambda_{\min}(P)$  and  $c_2 := \frac{1}{2}\lambda_{\max}(P)$ ,

$$c_1 \|z\|^2 \leq V(\tilde{g}, \eta) \leq c_2 \|z\|^2. \quad (35)$$

*Dissipation along the autonomous limit.* Fix an active set  $S$ . Along the autonomous system  $d\tilde{g}/d\tau = -(A_* + E_S)\eta$ ,  $d\eta/d\tau = \tilde{g} - \eta$  obtained by freezing  $A(x)$  at  $A_*$  and dropping the  $e^{-\tau}$  forcing in (34), Lemma 4 gives

$$\left. \frac{dV}{d\tau} \right|_{\text{auto}} = z^\top P M_S z \leq -\kappa_0 \|z\|^2, \quad (36)$$

with  $\kappa_0 = \kappa_0(A_*)$  from (29), uniform over all active sets.

**Step 3 (Decomposition along the true dynamics).** Fix the active set  $S$  and split the constraint matrix in (34) as  $A(x) = A_* + \Delta(x)$ ,  $\Delta(x) := A(x) - A_*$ . Differentiating  $V$  along (34) and the  $\eta$ -dynamics (33) and substituting this splitting,

$$\frac{dV}{d\tau} = \underbrace{z^\top P M_S z}_{\leq -\kappa_0 \|z\|^2 \text{ (36)}} \underbrace{- (\nabla_{\tilde{g}} V)^\top \Delta(x) \eta}_{=: R_\Delta} + (\nabla_{\tilde{g}} V)^\top \underbrace{\left( e^{-\tau} \left[ b - c(A(x) + E_S)\tilde{g} \right] - c e^{-\tau} s_{S^c} \right)}_{\text{forcing}},$$

where  $M_S$  is the autonomous matrix built from  $A_*$  and  $\nabla_{\tilde{g}} V = \tilde{g} - \frac{1}{2}\eta$ . As in the equality case, the deviation  $\Delta(x)$  enters only through the constraint block, and does so identically in every regime, since it shifts each  $A_* + E_S$  by the same amount.

*Bound on  $R_\Delta$  (Jacobian variation).* Using  $\|\nabla_{\tilde{g}} V\| \leq \frac{\sqrt{5}}{2} \|z\|$  from Lemma 4 and  $\|\Delta(x)\eta\| \leq \|\Delta(x)\|_2 \|\eta\| \leq \|\Delta(x)\|_2 \|z\|$ ,

$$|R_\Delta| \leq \frac{\sqrt{5}}{2} \|\Delta(x)\|_2 \|z\|^2 \leq \rho \|z\|^2,$$

where  $\rho = \frac{\sqrt{5}}{2} \sup_t \|\Delta(x_t)\|_2$  as in (30); for affine constraints  $\Delta \equiv 0$ , so  $R_\Delta = 0$ .

*Bound on the forcing.* By (B1),  $\|b\| \leq LB$ ; by (B2),  $\|A(x) + E_S\|_2 \leq a_{\max} + 1$ ; by (B3),  $\|\tilde{g}\| \leq \|h\| + \|s\| \leq G + S =: G'$  and  $\|s\| \leq S$ . Hence the forcing is bounded in norm by  $e^{-\tau} B_0$  with  $B_0 := LB + c(a_{\max} + 1)G' + cS$ , and by Cauchy–Schwarz,

$$(\nabla_{\tilde{g}} V)^\top (\text{forcing}) \leq e^{-\tau} \frac{\sqrt{5}}{2} B_0 \|z\| =: e^{-\tau} K \|z\|, \quad K = \frac{\sqrt{5}}{2} \left( LB + c(a_{\max} + 1)G' + cS \right).$$

*Combined inequality.* Collecting the three terms,

$$\frac{dV}{d\tau} \leq -(\kappa_0 - \rho) \|z\|^2 + e^{-\tau} K \|z\|, \quad (37)$$

with  $\kappa_0 - \rho > 0$  by the small-variation condition (30).

**Step 4 (Comparison lemma and explicit rate).** As in the equality case, the rescaled dual variable  $\eta = (1 - t)\lambda$  is not bounded a priori ((B3) bounds  $x_t$  and  $s_t$ , not  $\lambda_t$ ). The comparison lemma

produces the bound. Set  $y := \sqrt{V} \geq 0$ . Where  $V > 0$ ,  $\frac{dy}{d\tau} = \frac{1}{2\sqrt{V}} \frac{dV}{d\tau}$ ; bounding the dissipation term in (37) from below via  $\|z\|^2 \geq V/c_2 = y^2/c_2$  and the forcing term from above via  $\|z\| \leq \sqrt{V}/c_1 = y/\sqrt{c_1}$  (both from (35)),

$$\frac{dy}{d\tau} \leq \frac{1}{2y} \left[ -(\kappa_0 - \rho) \frac{y^2}{c_2} \right] + \frac{1}{2y} e^{-\tau} K \frac{y}{\sqrt{c_1}} = -\alpha y + \gamma e^{-\tau},$$

where  $\alpha := \frac{\kappa_0 - \rho}{2c_2} > 0$  and  $\gamma := \frac{K}{2\sqrt{c_1}} > 0$ . We are left with a scalar differential inequality for  $y$ . The comparison lemma [33, Lemma 3.4] implies that for all  $\tau \in [0, \infty)$

$$y(\tau) \leq y(0)e^{-\alpha\tau} + \gamma \int_0^\tau e^{-\alpha(\tau-u)} e^{-u} du = y(0)e^{-\alpha\tau} + \gamma \begin{cases} \frac{e^{-\alpha\tau} - e^{-\tau}}{1 - \alpha}, & \alpha \neq 1, \\ \tau e^{-\tau}, & \alpha = 1. \end{cases}$$

From this bound,  $y$  is bounded on  $[0, \infty)$ , so  $\|z\| \leq y/\sqrt{c_1}$  is bounded and in particular  $(1-t)\|\lambda_t\| = \|\eta\| \leq \|z\|$  stays bounded as  $t \rightarrow 1^-$ . Moreover  $y(\tau) \rightarrow 0$ . Moreover, the top-left block of  $P$  in Lemma 4 is  $I_k$ , so  $\lambda_{\max}(P) \geq 1$ , and with  $\kappa_0 \leq \frac{1}{2}$  and  $\rho \geq 0$  we have  $\alpha = (\kappa_0 - \rho)/\lambda_{\max}(P) \leq \kappa_0 \leq \frac{1}{2} < 1$ . Therefore, there exists a constant  $M > 0$  such that  $y(\tau) \leq M e^{-\alpha\tau}$  for all  $\tau \geq 0$ . Converting to original time via  $e^{-\tau} = 1 - t$ , and using  $\|\text{ReLU}(h(x_t))\| \leq \|\tilde{g}\| \leq \|z\| \leq y/\sqrt{c_1}$  (the first inequality by  $s_t \geq 0$ , Lemma 2),

$$\|\text{ReLU}(h(x_t))\| \leq \frac{M}{\sqrt{c_1}} (1-t)^\alpha = O((1-t)^\alpha) \quad \text{and} \quad (1-t)\|\lambda_t\| = \|\eta\| = O((1-t)^\alpha),$$

as  $t \rightarrow 1^-$ . In particular  $\|\text{ReLU}(h(x_t))\| \rightarrow 0$ , so the generated sample is feasible in the limit.  $\square$

We now prove Lemma 4.

*Proof of Lemma 4. Positive definiteness.* The top-left block of  $P$  is  $I \succ 0$ , and its Schur complement is  $(A_* + \frac{1}{2}I) - (\frac{1}{2}I)(\frac{1}{2}I)^\top = A_* + \frac{1}{4}I \succ 0$ , so  $P \succ 0$ .

*Dissipation.* A direct block computation gives  $M_E^\top P + PM_E = \begin{pmatrix} -I & I-E \\ I-E & E-A_*-I \end{pmatrix} =: D_E$ . The top-left block is  $-I \prec 0$ ; the Schur complement of  $D_E$  is

$$(E - A_* - I) - (I - E)(-I)^{-1}(I - E) = (E - A_* - I) + (I - E)^2.$$

Because  $E$  is a 0/1 diagonal projector,  $E^2 = E$ , hence  $(I - E)^2 = I - 2E + E^2 = I - E$ , and the Schur complement collapses to

$$(E - A_* - I) + (I - E) = -A_* \prec 0.$$

Thus  $D_E \prec 0$  for every  $E$ , with no condition on  $A_*$  beyond  $A_* \succ 0$  and no assumption relating  $E$  to  $A_*$ . Since the active sets  $\mathcal{S}$  form a finite set,  $\kappa_0 = \frac{1}{2} \min_{\mathcal{S}} \lambda_{\min}(-D_{E_{\mathcal{S}}}) > 0$ . Along the autonomous flow,  $dV/d\tau = z^\top PM_{\mathcal{S}}z = \frac{1}{2}z^\top D_{E_{\mathcal{S}}}z \leq -\frac{1}{2}\lambda_{\min}(-D_{E_{\mathcal{S}}})\|z\|^2 \leq -\kappa_0\|z\|^2$ , which gives the stated dissipation.

*Gradient bound.*  $\nabla_{\tilde{g}}V = \tilde{g} - \frac{1}{2}\eta$ , so by Cauchy-Schwarz,  $\|\nabla_{\tilde{g}}V\| \leq \|\tilde{g}\| + \frac{1}{2}\|\eta\| \leq \frac{\sqrt{5}}{2}\|(\tilde{g}, \eta)\|$ .  $\square$

## C Different Choices for $p$

In this section, we provide some more analysis for the equality-constrained case for  $p \neq 2$ . To summarize our results,

- For  $p \in [1, 2)$ , we show that the residual  $\|g(x_t)\|$  converges to a limit as  $t \rightarrow 1^-$ , but this limit is generally nonzero;
- $p = 2$  is the case studied in Theorem 1. We prove constraint satisfaction under Assumptions (A1)-(A4);

- For  $p > 2$ , we do not have general convergence results though analysis of a simplified scalar setting in Appendix C.2 indicates that we can see constraint satisfaction in this case.

To facilitate the presentation, we first present an essential change of coordinates. For  $p \in [1, \infty)$ , define

$$\eta(t) := (1-t)^{p-1} \lambda(t), \quad \tau := -\log(1-t), \quad (38)$$

so  $\tau \in [0, \infty)$  and  $1-t = e^{-\tau}$ . Note that when  $p = 1$ ,  $\eta(t) = \lambda(t)$ .

Using these new coordinates, our dynamics become

$$\frac{dx}{d\tau} = -e^{(p-2)\tau} \nabla g(x)^\top \eta + e^{-\tau} F(x, \tau), \quad (39)$$

$$\frac{d\eta}{d\tau} = g(x) - (p-1)\eta, \quad (40)$$

where  $F(x, \tau) := v_\theta(x, t(\tau)) - c \nabla g(x)^\top g(x)$ .

### C.1 $p \in [1, 2)$

The exponent  $p$  enters (39) only through the gain  $e^{(p-2)\tau}$  multiplying the dual correction, and this gain determines the steady-state behavior of these dynamics. At  $p = 2$  the gain is constant, and (39)-(40) approach an autonomous system as  $\tau \rightarrow \infty$ ; this is the setting of Theorem 1. For  $p > 2$  the gain grows without bound, resulting in increased numerical stiffness near  $t = 1$ . For  $p \in [1, 2)$ , by contrast, the gain decays exponentially in  $\tau$ . The following proposition makes this precise.

**Proposition 5.** *Let  $p \in [1, 2)$  and suppose Assumptions (A1)-(A3) hold along the trajectory of (8). Then there exists  $x_1^* \in \mathbb{R}^n$  such that  $x_t \rightarrow x_1^*$  as  $t \rightarrow 1^-$ , and hence  $g(x_t) \rightarrow g_1 := g(x_1^*)$ . The constraint is satisfied in the limit if and only if  $g_1 = 0$ , which the dynamics do not enforce.*

*Proof.* By Assumptions (A1) and (A3), there are constants  $G, L, B \geq 0$  with  $\|g(x_\tau)\| \leq G$ ,  $\|\nabla g(x_\tau)\|_2 \leq L$ , and  $\|F(x_\tau, \tau)\| \leq B + cLG =: M_F$  along the trajectory.

First we bound  $\eta$ . Solving the linear equation (40) by variation of constants, with  $\eta(0) = \lambda_0 = 0$ ,

$$\eta(\tau) = \int_0^\tau e^{-(p-1)(\tau-u)} g(x(u)) du,$$

so for  $p \in (1, 2)$  we get  $\|\eta(\tau)\| \leq G/(p-1)$  for all  $\tau$ , and for  $p = 1$  we get  $\|\eta(\tau)\| \leq G\tau$ .

Substituting these bounds into (39),

$$\left\| \frac{dx}{d\tau} \right\| \leq L e^{(p-2)\tau} \|\eta(\tau)\| + M_F e^{-\tau} =: \varphi(\tau),$$

and since  $p-2 < 0$ , the function  $\varphi$  is integrable on  $[0, \infty)$  in both cases.

Since  $dx/d\tau$  is bounded and integrable on  $[0, \infty)$ , the following integral is absolutely convergent which lets us define the limit

$$x_1^* := x_0 + \int_0^\infty \frac{dx}{d\tau} d\tau. \quad (41)$$

We can then see that  $\|x(\tau) - x_1^*\| \leq \int_\tau^\infty \varphi(u) du \rightarrow 0$  as  $\tau \rightarrow \infty$ . Therefore we conclude that  $x(\tau) \rightarrow x_1^*$  as  $\tau \rightarrow \infty$  (or equivalently that  $x_t \rightarrow x_1^*$  as  $t \rightarrow 1^-$ ) and that  $g(x_t) \rightarrow g(x_1^*)$  as  $t \rightarrow 1^-$  by continuity.  $\square$

We exhibit a simple instance in which the failure described by Proposition 5 can be established by a direct argument in the  $\tau$ -coordinates. Let  $n = m = 1$  with  $g(x) = x$ , and take  $v_\theta = 0$  and  $c = 0$ : the flow has no drift and no penalty, so the dual variable is the only mechanism acting on the sample, and its only task is to bring  $x$  to the constraint set  $\{x = 0\}$ . With  $p = 1$  we have  $\eta = \lambda$ , and the general dynamics (39)-(40) become the simple system

$$\frac{dx}{d\tau} = -e^{-\tau} \eta, \quad \frac{d\eta}{d\tau} = x, \quad x(0) = x_0, \quad \eta(0) = 0, \quad (42)$$

where  $\tau = \log \frac{1}{1-t} \in [0, \infty)$  and constraint satisfaction as  $t \rightarrow 1^-$  corresponds to  $x(\tau) \rightarrow 0$  as  $\tau \rightarrow \infty$ .

Integrating the two equations of (42) from 0 gives the two identities

$$\eta(\tau) = \int_0^\tau x(u) du, \quad x(\tau) = x_0 - \int_0^\tau e^{-u} \eta(u) du. \quad (43)$$

**Proposition 6.** *Let  $x_0 > 0$ . Along (42),  $x(\tau) > 0$  and is strictly decreasing for all  $\tau > 0$ , and*

$$x_\infty := \lim_{\tau \rightarrow \infty} x(\tau) \text{ exists with } 0 < x_\infty \leq \frac{1}{2}x_0.$$

*Hence  $x_\infty \neq 0$  whenever  $x_0 \neq 0$ , and the constraint is not satisfied in the limit.*

*Proof.* We will use the following fact several times:

$$\int_0^\infty u e^{-u} du = 1. \quad (44)$$

First we show that when  $x_0 > 0$ , we have that  $x_\tau > 0$  for all  $\tau > 0$ . To this end, let  $\tau^* := \sup\{T \mid x(u) > 0 \text{ for all } u \in [0, T]\}$ , which is positive since  $x(0) = x_0 > 0$  and  $x$  is continuous. On  $[0, \tau^*)$  we have  $x > 0$ , so by the first identity in (43)  $\eta > 0$ , hence  $dx/d\tau = -e^{-\tau}\eta < 0$ : the residual is strictly decreasing, and in particular  $x(u) < x_0$  for  $u \in (0, \tau^*)$ . Therefore  $\eta(u) = \int_0^u x(r) dr < x_0 u$  for every  $u \in (0, \tau^*)$ , and the second identity in (43) gives, for any  $\tau \in (0, \tau^*)$ ,

$$x(\tau) = x_0 - \int_0^\tau e^{-u} \eta(u) du > x_0 - x_0 \int_0^\tau u e^{-u} du > x_0 - x_0 \int_0^\infty u e^{-u} du = 0,$$

using (44) in the last step. Thus  $x$  is bounded away from zero on every compact subinterval and can never reach it, so  $\tau^* = \infty$ : the residual stays positive and strictly decreasing for all  $\tau$ .

Being positive and strictly decreasing,  $x(\tau)$  has a limit  $x_\infty \in [0, x_0)$ . Since  $x(r) < x_0$  for every  $r > 0$ , the strict inequality  $\eta(u) < x_0 u$  holds for all  $u > 0$ . Multiplying by the positive weight  $e^{-u}$  and integrating over  $(0, \infty)$ ,

$$\int_0^\infty e^{-u} \eta(u) du < x_0 \int_0^\infty u e^{-u} du = x_0.$$

Letting  $\tau \rightarrow \infty$  in the second identity of (43) therefore yields

$$x_\infty = x_0 - \int_0^\infty e^{-u} \eta(u) du > x_0 - x_0 = 0.$$

For the upper bound,  $x(u) \geq x_\infty$  gives  $\eta(u) \geq x_\infty u$ , hence  $\int_0^\infty e^{-u} \eta(u) du \geq x_\infty$  by (44), so  $x_\infty = x_0 - \int_0^\infty e^{-u} \eta \leq x_0 - x_\infty$ , i.e.  $x_\infty \leq \frac{1}{2}x_0$ . The case that  $x_0 < 0$  is handled by symmetry and is omitted.  $\square$

## C.2 $p > 2$

To provide supporting evidence that we can see constraint satisfaction for  $p > 2$ , we revisit the scalar example from the previous section ( $n = m = 1$ ,  $g(x) = x$ , and  $v_\theta = 0$ ). Using the same change of coordinates  $\tau = -\log(1-t)$  and  $\eta = (1-t)^{p-1}\lambda$ , we are left with the coupled system

$$\frac{dx}{d\tau} = -e^{(p-2)\tau} \eta, \quad \frac{d\eta}{d\tau} = x - (p-1)\eta, \quad x(0) = x_0, \quad \eta(0) = 0. \quad (45)$$

Differentiating the first equation and substituting the second turns (45) into a single scalar equation for the residual,

$$\frac{d^2x}{d\tau^2} + \frac{dx}{d\tau} + e^{(p-2)\tau} x = 0, \quad x(0) = x_0, \quad \frac{dx}{d\tau}(0) = 0, \quad (46)$$

which is a damped oscillator with unit damping and a stiffness  $e^{(p-2)\tau}$  that grows unbounded when  $p > 2$ . Constraint satisfaction as  $t \rightarrow 1^-$  is the statement  $x(\tau) \rightarrow 0$ . Note that when  $p = 2$ , this

is a standard damped oscillator whose solution trajectories tend to the origin exponentially quickly, agreeing with the results of Theorem 1.

First, we will choose the substitution  $x(\tau) = e^{-\tau/2}y(\tau)$ . Computing the derivatives of  $x(\tau)$  and substituting them into the equation (46), we get the differential equation for  $y$ :

$$\frac{d^2y}{d\tau^2} + \left( e^{(p-2)\tau} - \frac{1}{4} \right) y = 0. \quad (47)$$

Let  $Q(\tau) = e^{(p-2)\tau} - \frac{1}{4}$ . Since  $p > 2$ , we see that  $Q$  is strictly positive and non-decreasing, i.e.,  $Q(\tau) > 0$  and  $Q'(\tau) \geq 0$ . Going forward, we will use  $'$  to denote a derivative with respect to  $\tau$ .

Define the energy function

$$V(\tau) = \frac{1}{Q(\tau)}(y')^2 + y^2. \quad (48)$$

Since  $Q(\tau) > 0$ ,  $V(\tau)$  is always nonnegative and satisfies that  $y^2 \leq V(\tau)$ , meaning that if we can show that  $V$  is bounded, we will conclude that  $y$  is as well. Taking a  $\tau$ -derivative of  $V$  yields

$$\begin{aligned} \frac{dV}{d\tau} &= \frac{2y'y''Q(\tau) - (y')^2Q'(\tau)}{Q(\tau)^2} + 2yy' = \frac{-2yy'Q(\tau)^2 - (y')^2Q'(\tau)}{Q(\tau)^2} + 2yy' \\ &= -\frac{Q'(\tau)}{Q(\tau)^2}(y')^2 \leq 0. \end{aligned}$$

Therefore, for all  $\tau \in [0, \infty)$ , we have that  $V(\tau) \leq V(0)$ . Since  $y^2(\tau) \leq V(\tau)$ , we conclude that  $y$  is bounded and cannot grow to infinity. Mapping back to  $x$ ,  $|x(\tau)| = e^{-\tau/2}|y(\tau)| \rightarrow 0$  as  $\tau \rightarrow \infty$ . Therefore, we get constraint satisfaction in this case for any initial condition and any  $p > 2$ .